J. Applied Membrane Science & Technology, Vol. 28, No. 2, August 2024, 27–47

A Comprehensive Examination of Low GO-Silica Loading in Pebax1657/PEI Thin Film Nano-composite Membranes for Gas Dehydration

A. R. Valagohar, S. A. Hashemifard*, M. A. Ghanavatyan & A. Khosravi

Sustainable Membrane Technology Research Group (SMTRG), Faculty of Petroleum, Gas and Petrochemical Engineering (FPGPE),
Persian Gulf University (PGU), P.O. Box 75169-13798, Bushehr, Iran

Submitted: 20/4/2024. Revised edition: 26/5/2024. Accepted: 27/5/2024. Available online: 22/7/2024

ABSTRACT

The aim of this study was to assess the effectiveness of blending Pebax1657 polymer with SiO_2-GO nanoparticles in the production of TFN membranes for N_2 gas dehydration. By utilizing dip coating, nanoparticles were incorporated at varying concentrations. The resulting nanocomposites were subjected to thorough analysis to investigate their chemical structure, physical morphology, surface topology, and thermal stability. This examination encompassed the application of FTIR, SEM, CA, AFM, and TGA techniques. The results demonstrated that the samples displayed good thermal stability and a highly hydrophilic surface. The investigation concluded that the dehydration properties of TFN membranes are influenced by a variety of factors, such as morphology, plasticization, and hydrophilic attributes. The effectiveness of the system is contingent upon the contribution made by each individual nanoparticle. The impact of SiO_2 nanoparticles in their pure form is clearly evident in the 0.5 wt% loaded composite membrane membrane. When 0.5% of SiO_2 nanoparticles are introduced into the composite membrane, the morphology closely resembles the ideal state due to the non-porous nature of SiO_2 and the low concentration of nanoparticles, hence a selectivity of ~560 is experienced. Fortunately this selectivity is beyond the need of the industries. Consequently, there was a reduction in water vapor and nitrogen permeability, resulting in a heightened selectivity ratio. These discoveries hold considerable importance in industrial settings, as they offer a more comprehensive understanding of the topic.

Keywords: TFN, TFC, Dehydration, Graphene Oxide (GO), SiO_2

1.0 INTRODUCTION

Existing in underground reservoirs with oil and water, natural gas is an essential primary energy source that operates under specific temperature and pressure conditions. Water vapor, among other impurities, poses a significant challenge as it can condense and solidify into gas hydrates, causing blockages in pipelines and control systems. Eliminating water vapor from pipelines not only mitigates corrosion and the potential for hydrate formation and freezing but also amplifies the heating efficiency of the gas [1]. Gas desalination can be achieved using different industrial-scale methods, such as liquid absorption, adsorption, the Twister Separator System, and membrane processes [2, 3].

In membrane processes, substances are separated by a thin selective layer that controls mass transfer. The selectivity of the membrane is achieved through mechanisms such as Knudsen diffusion, molecular sieve, solution-diffusion, surface diffusion, and

* Corresponding to: S. A. Hashemifard (email: salhashemifard@yahoo.com)
DOI: https://doi.org/10.11113/amst.v28n2.294

capillary condensation, which vary based on the structure. Solution-diffusion stands as the key mechanism for the separation of small gases like natural gas components [4]. This model is based on a non-porous selective layer that enables separation by exploiting differences in solubility and diffusion across the membrane [5, 6].

The membrane's permeability and selectivity are the key attributes to consider. Gas separation membranes are manufactured in two forms: flat plate and hollow fiber, primarily used in natural gas separation applications. Hollow fiber membranes, due to their larger surface area per unit volume and resistance to fouling, exhibit greater suitability for gas separation [7]. It is apparent that gas separation demands membrane materials that possess both high permeability and selectivity.

As the condensability of gas and vapor increases, their solubility generally follows suit. This relationship is determined by factors like critical temperature or Lennard-Jones temperature. Water, with its higher density and significantly higher critical temperature or Lennard-Jones temperature, outperforms uncondensable gases like methane or nitrogen in terms of solubility. Conversely, smaller molecular size, as indicated by a smaller critical volume or kinetic diameter, enhances gas penetration. In comparison, water molecules (with a critical volume of 1.57 or kinetic diameter of 2.6 A) are smaller than methane molecules (with a critical volume of 2.99 or kinetic diameter of 3.8 A) [8].

Lin *et al*. [8, 9] conducted a study on process simulation to assess various designs for H_2O/CH_4 separation. The design using dry gas as a sweeping gas in the permeation section showed the best results with the least membrane surface area required. Gas permeability and selectivity were tested at 35 bar and 27°C, suggesting that membrane processes with sweeping gas could rival glycol-based dehumidification. Suggestions to improve gas permeability and selectivity include developing new polymers, enhancing existing ones, using membrane copolymers, and advancing thin film composite (TFC), thin film nanocomposite (TFN), and mixed matrix membranes (MMM).

A composite membrane consists of different polymers with a selective upper layer on a porous substrate. Membranes are effective in gas separation due to their thinness, cross-linked connections, and high upper layer density. Hashemifard *et al*. [10] investigated water vapor separation from a wet gas stream using a TFC hollow fiber membrane. Increasing meta-phenylene diamine (MPD) concentration increased water vapor flux, while increasing tri-mesoyl chloride (TMC) concentration reduced nitrogen gas permeability and increased selectivity. Even a small amount of water vapor in the feed had a significant impact on permeability compared to its pure form. The plasticization effect of H_2O had a stronger influence on nitrogen penetration than water vapor. Modeling showed higher water vapor penetration due to lower D_{N2} compared to D_{H2O}. The composite membrane analyzed by Do *et al* [11] consisted of a hydrophilic polymer polyacrylonitrile (PAN) substrate and an active layer of polydimethylamino methacrylate (PDMAEMA). The researchers noted that the PAN substrate had minimal impact on methane permeability, whereas the novel hydrophilic active layer greatly enhanced water vapor permeability. Generally, membranes possessing hydrophilic properties are favored for their ability to absorb water vapor. The properties of a hydrophilic hollow fiber composite membrane composed of sulfonated Poly(Ether

Ether Ketone) and polyethersulfone (SPEEK/PES) were investigated by Chen *et al*. [12]. Their study demonstrated the impressive thermal stability and mechanical properties of SPEEK/PES hollow fiber composite membranes for exhaust gas dehumidification. Furthermore, the researchers examined the impact of gas flow rate and feed gas temperature on the separation of water vapor/nitrogen. The findings revealed that as the temperature elevated from 40°C to 70°C, the permeability of water vapor also experienced an increase.

Cong *et al*. [13] studied the use of zeolite NaA nanoparticles in the polyamide layer to create a TFN membrane. Other nanoparticles such as SiO_2, silver, graphene oxide (GO), alumina, and TiO_2 have also been incorporated by researchers to improve TFC efficiency. Dip coating and interfacial polymerization are commonly used techniques for manufacturing thin film and nanocomposite thin film membranes [14-16]. Baig *et al*. [17] developed a TFN membrane by blending carboxylated TiO_2 nanoparticles into the polyamide matrix, resulting in increased hydrophilicity and improved water vapor permeability and selectivity. In another study by Baig *et al*. [18], GO and graphene oxide-TiO_2 (GT) nanoparticles were added to the selective layer of TFN membranes, showing strong bonding to the polyamide layer through hydrogen and covalent bonds. Kim *et al*. [19] found that Pebax polymers have distinct gas permeability characteristics due to the presence of impermeable regions like the hard polyamide part and regions with higher permeability like the flexible polyether blocks [20, 21]. Akhtar *et al*. [23] used Pebax® 1657 and graphene oxide nanosheets to decrease gas permeability and improve water molecule permeability. Even a small concentration of 2% GO nanoparticles in the Pebax layer led to a 12% reduction in water vapor permeability and a 70% decrease in nitrogen gas permeability, resulting in eightfold higher selectivity. Poormohammadian *et al*. [24, 25] studied water vapor permeability by adding silica and titania nanoparticles to Pebax 1657 polymers. Silica nanoparticles increased methane permeability more than water, reducing selectivity, while titania nanoparticles led to higher pure methane permeation rates due to higher FFV, resulting in lower selectivity compared to membranes with silica.

The inclusion of hydroxyl and carboxyl groups in GO has garnered attention due to their ability to form hydrogen networks with water molecules. However, there is a lack of research on using Pebax® polymer in producing composite membranes for dehydration. Hollow fiber membranes, with mechanical self-supporting properties and a larger surface area, are more suitable for dehydration than flat plate membranes. Additionally, the combined effect of graphene oxide and silica nanoparticles in creating TFN membranes has not been extensively studied. To address this gap, this study used a composite membrane made of polyetherimide (PEI) and Pebax® 1657 polymer, incorporating graphene oxide and silica nanoparticles to form TFN membranes for gas dehydration. The study focused on investigating how the addition of nanoparticles (including both GO and silica) influence the morphology, structural parameters, hydrophilicity, roughness, and separation properties of the TFN membranes in a dehydration process.

2.0 EXPERIMENTAL

2.1 Chemicals

The Polyetherimide PEI, commercially known as Ultem® 1000, was acquired from the American-based GE plastic company and processed accordingly. Pebax polymer 1657, manufactured by the French company Arkema, was also prepared. The procurement of n-methyl-2-pyrrolidone (NMP) as a solvent was carried out from Merck, Germany, due to its remarkable affinity towards polymers and commendable chemical durability. Throughout this study, a solvent of 96% purity ethanol was utilized for the synthesis of the Pebax 1657 polymer-containing layer. Furthermore, ethanol was used as an additive in the polymer solution to decrease thermodynamic stability and enhance porosity. The ethanol used in this research was produced by Lian Sun Co., Iran. Additionally, Tetraethylorthosilicate, officially known as TEOS, with a weight purity of 99%, was procured from Merck.

2.2 Fabrication of PEI Sublayer

The polymer solution was formulated by combining 15% by weight of PEI, 4% by weight of ethanol as a pore former agent, and 81% NMP as the solvent. The mixture was thoroughly mixed and agitated until it was completely homogenized. Subsequently, the polymer solution was continuously stirred for a duration of 24 hours using a hot plate magnetic stirrer to attain a uniform and transparent consistency. The dissolutions were carried out exclusively at a temperature of 60°C. Subsequently, the PEI polymer solution underwent a meticulous 2-hour ultrasonication process to effectively eliminate any potential bubbles that may have formed during the mixing procedure. Following this, the hollow fiber membranes were produced using a dry/wet spinning technique. The prepared polymer solution was poured into a syringe, while another syringe was employed to introduce distilled water as an internal coagulant. With the aid of a syringe pump, the polymer solution was then pumped to the spinneret at room temperature, maintaining a constant flow rate. Simultaneously, the internal coagulant (distilled water) was introduced into the spinneret using another syringe pump. The coagulation bath for the membranes utilized tap water. To ensure the solvent was completely eliminated from the fabricated membranes, they were immersed in water for three days and nights. The water was consistently replaced to ensure thorough removal of the solvent. The spinning conditions for the polyetherimide substrate membrane using hollow fiber technology were as follows: The polymer solution composition consisted of 15% PEI, 4% ethanol (EtOH), and 81% N-methyl-2-pyrrolidone (NMP). The bore fluid used was distilled water, with an inner diameter to outer diameter ratio of 0.6:0.42. The external coagulation fluid was tap water. The polymer solution flow rate was 4.5 cm^3/min, and the air gap was set at 5 cm. The bore fluid flow rate was 1.7 cm^3/min, and the fiber forming temperature was maintained at 24°C.

2.3 Synthesis of Active layer

The process of preparing a 3 wt% solution of Pebax 1657 involved dissolving the polymer in half of the solvent, which consisted of 70% ethanol and 30% water, at a temperature of 80 °C under reflux for a duration of 12 hours. Simultaneously, in a separate container, varying quantities of graphene oxide were mixed with the remaining half of the same solvent and

stirred for 2 hours at 45°C. The synthesis of graphene oxide nanoparticles was accomplished using the Hummer method [23]. Furthermore, diverse amounts of TEOS were blended with the 3% weight solution of Pebax 1657 at a temperature of 45°C for 2 hours. Afterward, the TEOS and Pebax 1657 solution were slowly incorporated into the graphene oxide solution and mixed for 2 hours at 60°C. To disperse graphene oxide and/or SiO_2 nanoparticles, the solution was subjected to a 2-hour treatment in an ultrasonic bath, followed by 20 minutes of ultrasonic stirring. Following that, the solution was allowed to remain at room temperature for a duration of 24 hours. In order to synthesize the composite membrane, the substrate PEI was immersed in the pre-prepared polymer solutions (Pebax 1657+nanoparticles). Subsequently, the coated membrane was retrieved from the container after 30-60 seconds and left to dry at a temperature of 40°C for a period of 24 hours. For comprehensive details on the material composition of the surface active layer and the corresponding codes for the produced membranes, please refer to Table 1.

Table 1 The codes of the fabricated membranes and the composition of materials in the active layer

Membrane M-P-GO%-SIO$_2$%	**Mix NPs wt. %**	**Pebax1657 wt. %**	**GO wt. %**	**SiO_2 wt.%**
M0-0	**0**	**0**	**0**	**0**
MP0-0	**0**	3	**0**	**0**
MP0.5-0	0.5	3	0.5	**0**
MP0.25-0.25	0.5	3	**0**.25	**0**.25
MP0-0.5	0.5	3	**0**	**0**.5

M0-0 is the substrate.

2.4 Characterization Methods

The gas permeability test device shown in Figure 1 provides a visual representation of the procedure for conducting the permeation of pure nitrogen gas. Initially, a 5.5 cm long hollow fiber membrane was carefully positioned and secured within a fitting using epoxy adhesive. Subsequently, the opposite end of the membrane was sealed with glue. The module glue was allowed to dry completely over a 24-hour period before being placed in a stanless steel cylinder and connected to a nitrogen gas cylinder with a purity level of 99.99. The pressure of the nitrogen gas passing through the outer side of the membrane was then raised incrementally from 0 to 6 bar gage, with a pressure difference of 0.5 bar. A bubble flowmeter was utilized to measure the gas permeation rate.

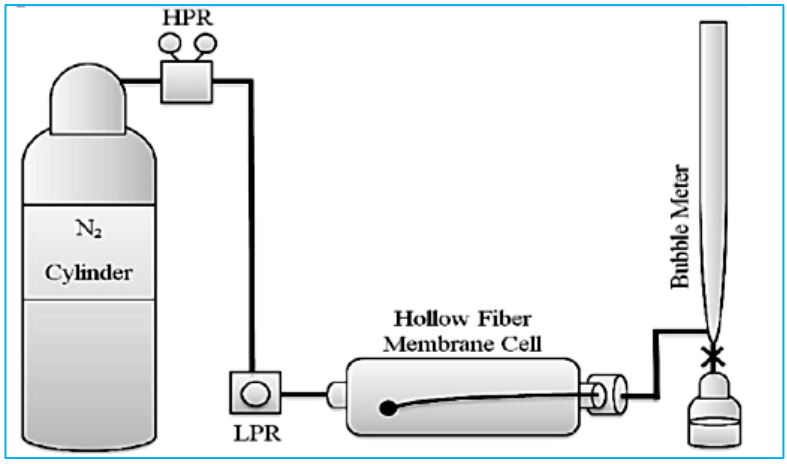

Figure 1 Gas Permeability Device Schematic

The gas permeability test is determined by various factors, such as the initial gas pressure at the inlet (Pa), the fixed volume of the bubble flow meter (V in ml), the time taken for gas to pass through the bubble flow meter at the fixed volume (t in seconds), and the length of the membrane (L in meters). These factors are essential in calculating the membrane permeability. Furthermore, the surface area (S) of the membrane is also considered, with the bore side area having a diameter (d) of 0.00045 meters.

Finally, the gas permeability (mol. m^{-2}. Pa^{-1}. s^{-1}) was obtained as follow:

$$P = \frac{101325}{8.314\times298\ \text{A}.\Delta\text{p}}\left(\frac{V}{t}\right) \quad (1)$$

Equation (2) was utilized to calculate the overall permeability by considering the combined gas permeability of Knudsen flow (P_k) and viscous flow (P_v) [10]. The assumption made was that the pores were straight and cylindrical in shape.

$$P = P_k + P_v = \left(\frac{2}{3}\right)\left(\frac{8\,RT}{\pi M}\right)^{0.5}\frac{r_{p.m}}{RT}\frac{\varepsilon}{Lp} + \frac{1}{8\,\mu}\frac{r_{\bar{p}.m}^2}{RT}\frac{\varepsilon}{Lp}\bar{p} = \text{A}+\text{B}\bar{\text{p}} \quad (2)$$

The mean pore radius (m), r_p (m), is used to calculate the average pressure on both sides of the membrane, $\bar{p}$. The universal gas constant (8.314 $J.mol^{-1}K^{-1}$), denoted as R, is involved in this calculation. The absolute temperature (K), represented by T, and the gas molecular weight (kg. $mol^{-1)}$, denoted as M, are also considered. Additionally, the gas viscosity (Pa. s), μ, the surface porosity, ε, and the effective pore length (m), Lp, are taken into account. By plotting P in terms of $\bar{p}$, the intercept (A) and slope (B) can be used to determine the mean pore size and surface effective porosity ε/Lp using equations (3) and (4) respectively [10].

$$r_{p.m} = \frac{16\text{B}}{3\text{A}}\left(\frac{8\,RT}{\pi M}\right)^{0.5}\mu \quad (3)$$

$$\frac{\varepsilon}{Lp} = \frac{8\text{RTB}}{r_{\bar{p}.m}^2} \quad (4)$$

The wettability of the hollow fiber membranes was examined through the implementation of a contact angle test. This test aims to determine the ability of water to make contact with the solid surface of the membrane, which is influenced by intermolecular forces. The extent of wetting is determined by the balance between cohesive and adhesive forces. The wetting angle for an ideal surface is defined by the Young-Laplace law:

$$\gamma_{SG} = \gamma_{SL} + \gamma_{LG}\cos\theta \quad (5)$$

The interfacial free energy between the liquid (L), solid (S), and gas (G) phases is denoted as γ in equation (12), whereas the contact angle is represented by θ.

The analysis conducted with an infrared spectrometer aids in the identification of organic substances and polymers, providing essential details on the chemical makeup of molecules, bonds, and functional groups found in the membrane structure. The FTIR-JASCO-4600, a Fourier-transform infrared spectroscopy machine made in Japan, was utilized for this examination. The assessment of particle size distribution in solutions and suspensions was conducted using DLS analysis, a physical technique. By analyzing the fluctuations in the intensity of scattered light rays, the particle size distribution was determined by considering the Brownian motion of the particles in the fluid phase. To determine the size of concentrated GO nanoparticles, a DLS device called Nano DS, manufactured by CILAS in France, was utilized in this research. Differential Thermal Gravimetric Analysis (TGA) was used to determine the thermal stability of the membranes produced from the thermal gravimetric test. The Perkin Elmer STA 6000 thermal analysis equipment was utilized in a nitrogen atmosphere for this purpose. During the experiment, samples weighing between 15 and 10 mg were subjected to heat treatment at a constant rate of approximately 10°C/min, starting from the ambient temperature and reaching 700°C. Utilizing the Scanning Electron Microscopy (SEM) test, the structure of the fiber membranes produced from the scanning microscopic radiation test was analyzed. Liquid nitrogen was used to break the samples in order to ensure a smooth surface. Subsequently, a thin layer of platinum was applied to enhance the samples' conductivity. The examination of the membrane structure was carried out using the TESCAN-Vega 3 SEM machine, which hails from the Czech Republic.

2.5 Gas Dehydration Experiment

Four modules containing several membranes were used to study the performance of the synthesized membranes, as detailed in Table 1. Each section was comprised of seven hollow fiber membranes that were 18 cm long. Following a comprehensive inspection to ensure the integrity of each membrane, the membrane section was assembled. Afterwards, the group of seven membranes was inserted into the steel shell sections, and both ends were securely attached using epoxy glue. After a day had passed for the glue to dry and ensuring the joints and membranes were secure, the edges of the detached membranes on both sides of the module were trimmed, exposing the openings completely. Subsequently, the module was set for testing. Initially, the membrane module was positioned in the gas dehydration equipment according to Figure 2. In order to generate steam and produce humid gas, the water temperature was raised by a heating element in an aluminum tank filled with water. This was carried out to transfer heat to the steel tank holding 250 milliliters of water. Dry nitrogen gas (N2 99.99 vol.%) was introduced into the steam generator chamber, where it came into contact with the steam and converted into wet gas at the outlet. The system was able to produce the desired gas with relative humidity percentage of 60% by adjusting the temperature inside the reservoir and generating a specific amount of steam. The humidity level of the nitrogen gas was measured using a digital portable humidity meter (TES-1360A made in Taiwan) upon entry and exit of the system. To determine the nitrogen

permeability a soap bubble flow meter was used and to determine the water vapor permeability the difference between the input wet gas and output dry gas was measured via the humidity meter and then the permeability was calculated. To determine the selectivity of the membrane, the input data for the calculations are as follow: inlet gas pressure, gas volume of the bubble in the flowmeter, gas bubble movement time, ambient and water vapor generator temperature, feed relative humidity, permeate relative humidity, retentate relative humidity, and feed flow rate. Finally, the selectivity was computed using equation (6) [10].

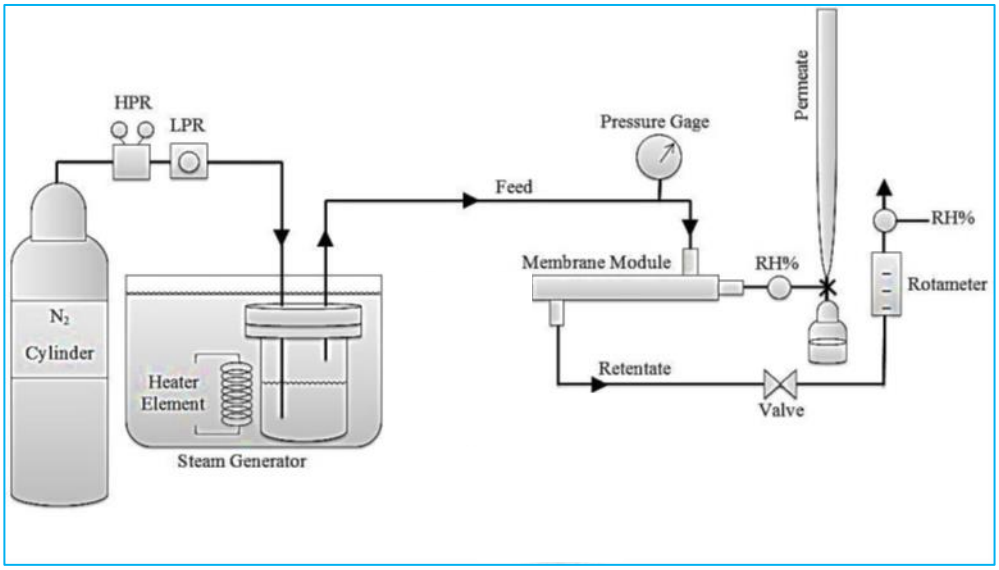

Figure 2 Gas dehydration device Schematic

$$\alpha = \frac{(Y^W/Y^G)}{(X^W/X^G)} \quad (6)$$

The mole fraction of water in the feed is denoted by X^W, while Y^W and Y^G signify the mole fractions of water and gas in the retentate. Further information on the material balance of the hollow fiber membrane module and the model derivation can be found in reference [10].

3.0 RESULTS AND DISCUSSION

3.1 Characterization for Synthesized GO Nanoparticles

The results of the FTIR analysis depicted in Figure 3 reveal the chemical and structural modifications that transpired during the production of graphene oxide from graphite. The FTIR spectrum of graphite exhibits a peak at 1635 cm^{-1}, which indicates the presence of C=C carbon double bonds. Subsequent to the synthesis of graphene oxide, additional peaks emerged at 1727-1056 cm^{-1}, confirming the existence of C-O and C=O bonds characteristic of graphene oxide. In the FTIR spectrum of graphene oxide, the peaks observed between the wavelengths of 3000-3600 cm^{-1} signify the existence of the OH group within the graphene oxide structure. The distinct peak of the OH group in the graphene oxide structure provides compelling evidence for the hydrophilic properties of graphene oxide and its excellent dispersibility in water. Additionally, the peak at 1727 cm^{-1}

corresponds to the C=O carbonyl group, indicating the presence of the carboxylic acid group on the surface of the graphene oxide nanoparticle. In addition, the peak identified at 1625 cm^{-1} is attributed to the carbon double bond, C=C. The modifications in the spectrum suggest the presence of carbonyl and hydroxyl groups in the chemical makeup, indicating the synthesis of graphene oxide.

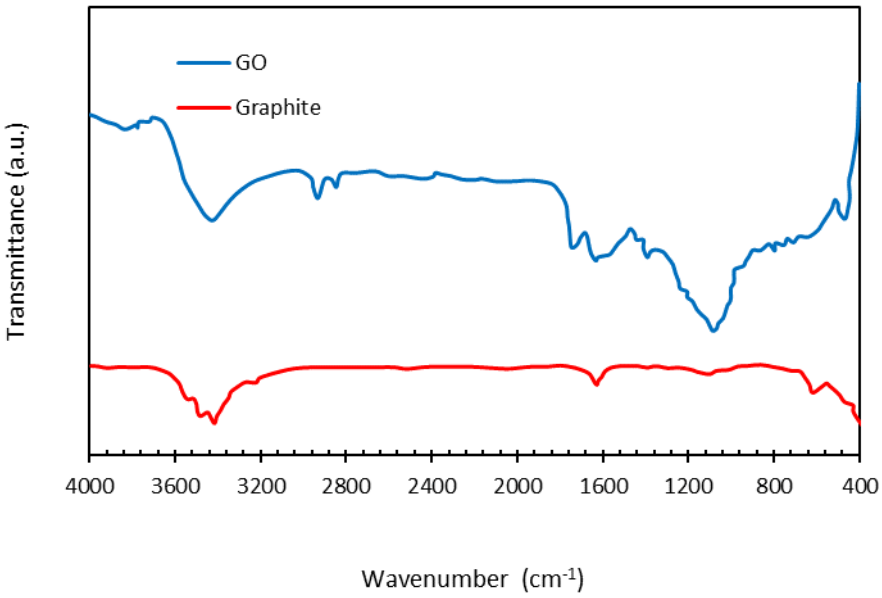

Figure 3 FTIR spectra of graphite and graphene oxide

The DLS analysis was conducted at a temperature of 25°C to determine the particle size of graphene oxide nanoparticles. The average dynamic diameter of these nanoparticles is found to be within the range of (95-100) nm.

3.2 Nitrogen Gas Permeability Results

Figure 4 displays the outcomes of the nitrogen gas permeability test conducted on the PEI substrate membrane. The results clearly demonstrate a progressive increase in permeance as the average gas pressure rises. In particular, the gas pressure has surged by 20 times, from 0.5 to 10 bar, resulting in a permeance alteration of 2.68×10^{-7} (mol/Pa.s.m^2). The sublayer membrane demonstrates an average gas permeability of 2.53×10^{-7} (mol/pa.s.m^2) within the examined pressure range. Furthermore, the porosity test reveals that the PEI substrate has a total porosity of approximately 81%. The mean pore size for the membrane sublayer is 222 nm, and the effective porosity is 3.49 m^{-1}.

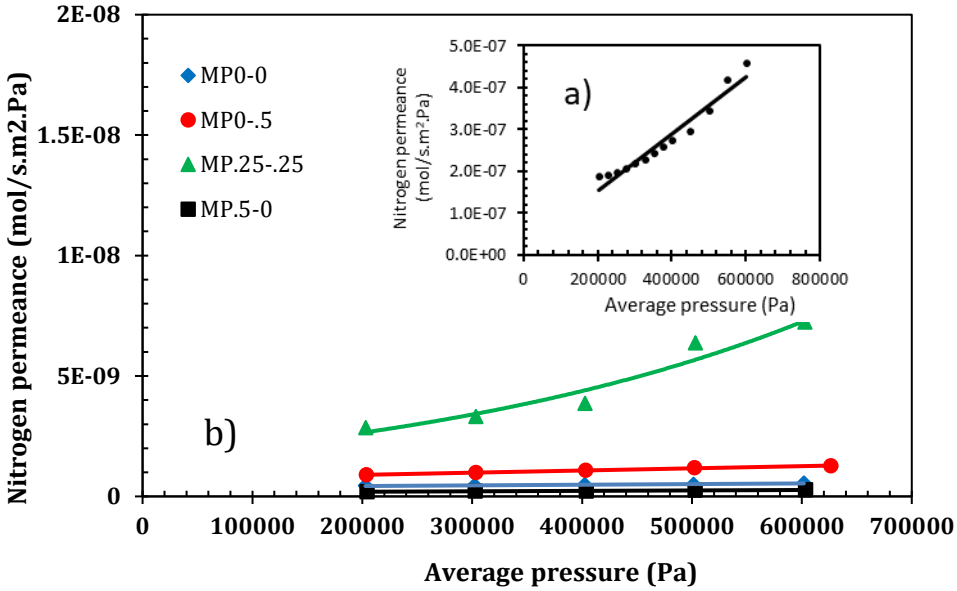

Figure 4 Nitrogen gas permeability of a) PEI sublayer, and b) TFN synthesized membranes as a function of average pressure, the correlation factor R2 was more than ~95%

The results of the nitrogen gas permeability test for TFN membranes are depicted in Figure 4. The figure provides a clear depiction of the noticeable decrease in nitrogen permeability experienced by membrane MP0-0, which was coated with Pebax1657 without nanoparticles. This decrease can be attributed to the penetration of the coating solution into the membrane pores, resulting in the formation of a dense active layer that effectively hinders the permeation of nitrogen. In the same manner, the rest of the membranes also showed significantly lower nitrogen permeation in comparison to the base membrane (i.e. substrate membrane), suggesting the development of a highly dense active layer on the substrate surface. The gas permeability decreased by nearly two orders of magnitude, which can be attributed to the creation of a dense active layer through the combination of Pebax 1657 polymer and nanoparticles like graphene oxide and SiO_2. The membrane M0.5-0 displayed the least permeability, indicating an optimal morphology. The introduction of SiO_2 led to an increase in nitrogen permeability, likely due to the emergence of a leaking morphology.

3.3 Contact Angle Results

The contact angle analysis evaluated the hydrophilicity of the produced membranes and the effect of the active layer composed of Pebax 1657 polymer, GO, and SiO_2 nanoparticles on the surface properties of TFN membranes. The results are provided in Table 2.

Table 2 The contact angle of the fabricated membranes

Membrane	Contact angle (°)
M0-0	78 ± 2
MP0-0	73 ± 2
MP0.5-0	19 ± 2
MP0.25-0.25	27 ± 2
MP0-0.5	31 ± 2

As per the Wenzel equation, the introduction of hydrophilic components and surface roughness enhances the hydrophilic characteristics of the

surface while reducing the contact angle. Nevertheless, the presence of minute air bubbles trapped between the roughness and water interface results in some hydrophobic properties, causing a slightly lower than anticipated decrease in the contact angle. The data in Table 2 underscore the relatively hydrophobic nature of the PEI substrate membrane. By incorporating a 3% Pebax1657 polymer active layer, the contact angle for MP0-0 decreased from its peak value of 78° to 73°, thereby enhancing the surface hydrophilicity in accordance with the Wenzel equation. Furthermore, the introduction of 0.5% graphene oxide nanoparticles to the MP0.5-0 membrane increased the surface hydrophilicity. Similarly, the inclusion of 0.5% SiO_2 nanoparticles in the active layer (MP0-0.5) enhanced the surface hydrophilicity, albeit not to the same extent as the membrane MP0-0, owing to the higher hydrophilicity of SiO_2 at elevated concentrations. Liu *et al.*'s study [26] indicates a potential correlation between GO and SiO_2 via covalent bonds involving (GO)-COOH and (Si-OH) (SiO_2), resulting in the alteration of functional groups containing hydrophilic oxygen and the formation of bonds as Si-O-C. This modification boosts hydrophilicity by reducing the SiO_2 concentration.

The contact angle of the Pebax1657 active layer was significantly influenced by the presence of nanoparticles, regardless of their type, quantity, and timing of addition. This resulted in an increased hydrophilicity of the membrane surface. The introduction of nanoparticles not only improved the surface hydrophilicity compared to the substrate and neat membrane MP0-0, but also increased the surface roughness. However, the combined effect of these two factors led to a decrease in the contact angle. The best outcomes were achieved with a lower amount of SiO_2, specifically 0.5% in total.

3.4 FTIR Results of Sublayer and PEI/Pebax Composite Membranes

The FTIR analysis of the PEI substrate and Pebax 1657 TFN membrane in Figure 5 revealed significant peaks indicating the presence of PEI polymer. The PEI polymer chain showed strong peaks at 1778 and 1721 cm-1 for the carbonyl imide group, as well as peaks for C-N bond stretching and bending at 1356 and 744 cm-1. A peak at 1236 cm-1 indicated C-O-C presence. Each segment of the Pebax 1657 copolymer displayed unique peaks in the FTIR spectrum, with peaks corresponding to polyamide and polyether components. The presence of these peaks in the MP0-0 membrane confirms successful application of the Pebax1657 coating on the PEI substrate, consistent with previous research by Kim *et al.* [27, 28].

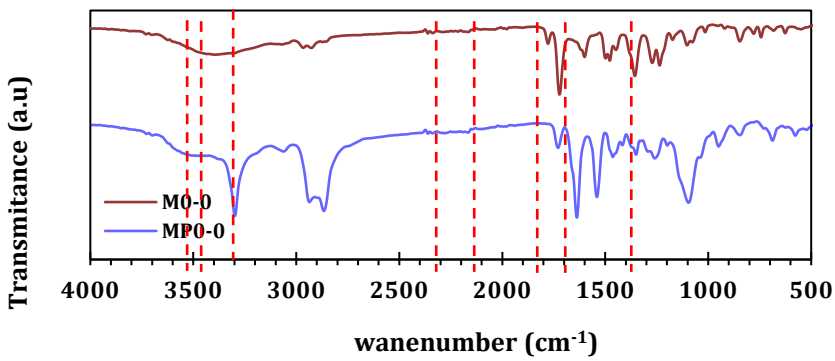

Figure 5 FTIR spectra for the sublayer membrane and the Pebax1657 coated membrane

3.5 FTIR Results of TFN Membranes

Figures 6 show the FTIR spectrum of thin layer nanocomposite membranes containing 0.5% GO/SiO_2 nanoparticles. The characteristic bands of GO are found at 1404 cm^{-1}, 1624 cm^{-1}, and 3410 cm^{-1}, corresponding to the bending vibration of -COOH, the bending vibration of -C=C- bond, and the stretching vibration of -OH, respectively. The coated membrane of 1657Pebax with varying amounts of GO nanoparticles does not exhibit any noticeable difference in the FTIR spectrum. This indicates that the peaks of graphene oxide nanoparticles align with those of 1657Pebax, as supported by references [29]. However, only the OH peak is observable due to the low concentration of GO in the skin layer, decreasing from 0.5% to zero loading. These observations suggest a good compatibility between GO and Pebax, attributed to hydrogen-bonding interaction. However, the situation changes with SiO_2 nanoparticles. It means that, SiO_2 nanoparticles exhibit distinct peaks at wavenumbers 1110-1020 cm^{-1}, 960 cm^{-1}, and 474 cm^{-1}, corresponding to the stretching and bending vibrations of Si-O-Si, Si-OH, and Si-O, respectively [30, 31]. As the percentage of SiO_2 nanoparticles increased, a noticeable increase in intensity was observed at 474 cm^{-1} in the spectrum of the samples. This peak serves as an indication of the presence of SiO_2 in the active layer. The influence of the nanoparticles loading in the active layer is clearly manifested through the intensity and strength of the peaks.

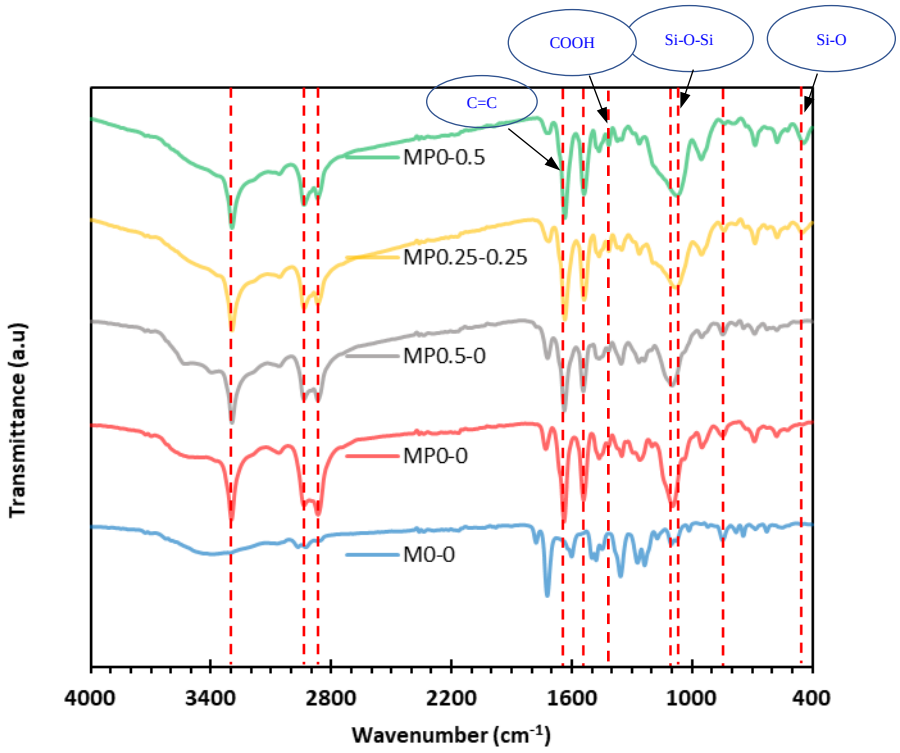

Figure 6 FTIR spectra for the TFN membranes containing 0.5% nanoparticles

3.6 TGA Analysis of Sublayer and 1657Pebax TFC Membranes

The DTG-TGA analysis of the substrate membrane and its Pebax1657 coating is illustrated in Figure 7. The results presented in the figure demonstrate a two-stage thermal degradation process. Initially, there is a weight loss of M0-0 between 50 to 140°C, which is due to the presence of moisture within the polymer chains. Subsequently, a slight weight loss is observed up to approximately 440°C, with the system remaining relatively stable within this temperature range. However, between 440 to 660°C, a significant weight loss occurs, indicating the degradation of the polymer chains.

Furthermore, the membrane MP0-0 exhibits an initial reduction in weight of approximately 3% within the temperature range of 110 to 130°C, which is likely attributed to the presence of moisture in the membrane structure. The weight loss process enters its second phase once the temperature reaches 300°C, signifying the onset of degradation. This phase primarily involves the degradation of the Pebax1657 polymer in the active layer. The degradation occurs due to the thermal decomposition of the amorphous portion of the polymer, resulting in a decrease in the degradation onset temperature compared to the pure substrate (M0-0). Subsequently, a significant weight loss persists between 480 and 660°C, which can be ascribed to the degradation of the PEI polymer chains within the substrate.

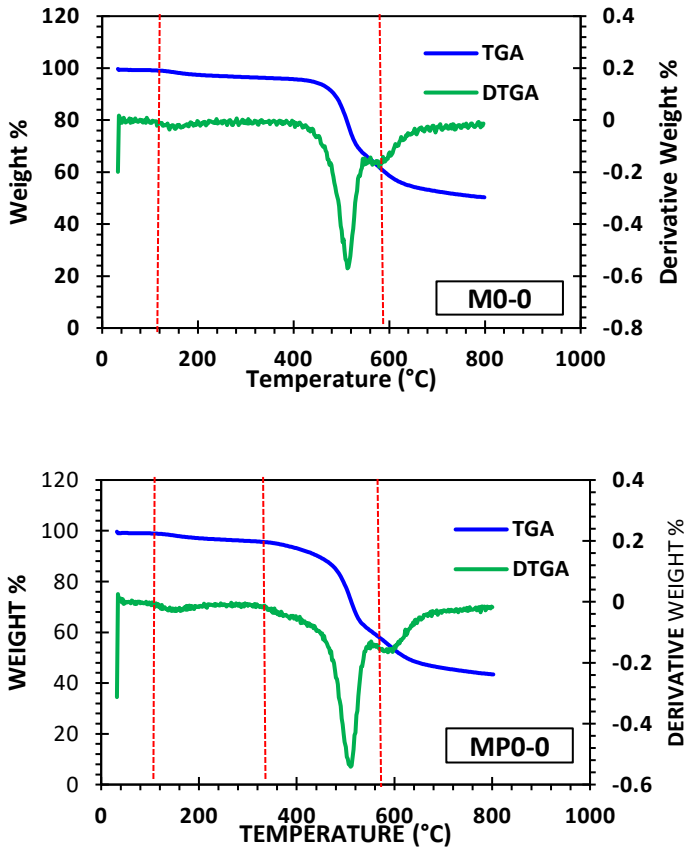

Figure 7 TGA-DTG results for the PEI substrate and Pebax 1657 TFC membrane

3.7 TGA Analysis of 1657Pebax TFN Membranes

The DTG-TGA analysis of TFN membranes in Figure 8 shows that all membranes lost weight initially from 30 to 130°C due to absorbed water release. Adding 0.5-1% nanoparticles lowered the degradation starting temperature from 510 to 480°C compared to the neat state. The MP0.5-0 membrane had weight reduction at 400-430°C from unstable oxygen groups in graphene oxide, and significant weight loss at 480-500°C from polymer decomposition. The MP0.25-0.25 membrane showed weight loss from 130-400°C due to increased unstable oxygen groups, weakened thermal strength, and improved hydrophilic property. This led to an increased degradation rate with temperature. Between 400-520°C, weight loss was attributed to polymer chains [32, 33].

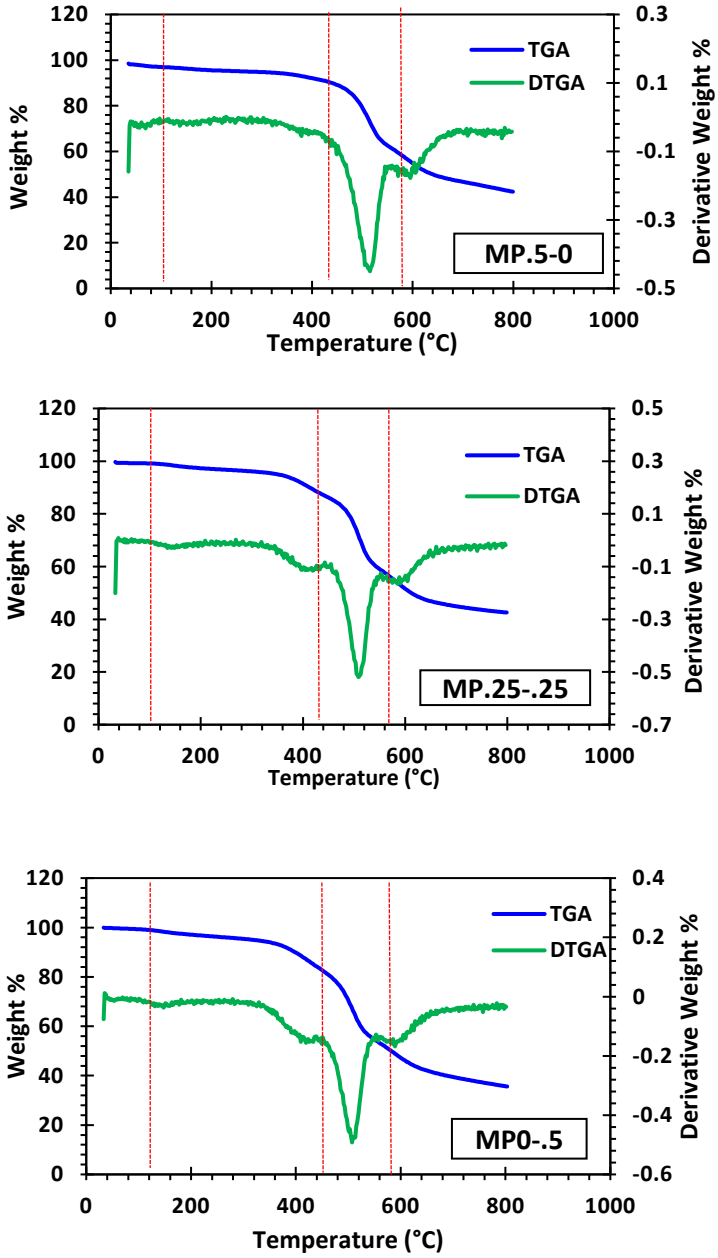

Figure 8 TGA-DTG results for the TFN fabricated membranes

The presence of SiO_2 nanoparticles (MP0-0.5) did not affect weight reduction within the tested temperature range. The graphs show that the membranes transform into carbon between 700-600°C. Overall, regardless of nanoparticle type and quantity, the decomposition temperature remained relatively unchanged, and the membranes exhibited good thermal stability within our study's temperature range.

3.8 Morphological Study

Figures 9 show the SEM spectrum of thin layer nanocomposite membranes with 0.5% loading of GO/SiO_2 nanoparticles. The cross-section of sublayer M0-0 is visible in both Figure 9A and 9a, with Figure 9a showing a magnified view of the substrate cross-section at a factor of ×2k. The substrate membrane has a thin and dense skin layer, with a blend of finger-like and open structures, along with a finely porous sponge-like structure. This porous configuration, with 81% porosity, reduces resistance for gas molecule transfer. Tear-like pores and a spongy formation are visible in certain areas. Figure 9B-b displays the outer surface of the Pebax1657-coated membrane and a cross-sectional segment of the MP0-0 membrane. According to the images, it is evident that the active layer, which comprises of Pebax1657, has undergone a growth in thickness in comparison to the M0-0 sublayer, almost an increment of 2.7 μm. The Pebax1657 layer displayed a compact, even, and flawless surface, devoid of any pores or imperfections. Since the same substrate was used for all TFN membranes, it was expected that the cross-sectional shape and structure would be consistent. Figure 9 C-c displays the surface and cross-section of the thin film nanocomposite membrane at MP0-0.5 with SiO_2 nanoparticles altering the surface morphology. SiO_2 nanoparticles are evenly dispersed in the active layer in Figures 11h. The active layer thickness is around 3-4 μm. SEM images show no abnormalities, indicating a flawless appearance. The secure attachment between the polymer and GO nanosheets is due to the flexible polymeric continuous phase and pliable components. GO nanoparticles are incorporated in the TFC active layer through hydrogen bonding interactions. The presence of nanoparticles results in a lighter phase, while the polymer matrix contributes to a darker phase. The outer surface of the membranes appears compact, while the cross-section is fully porous.

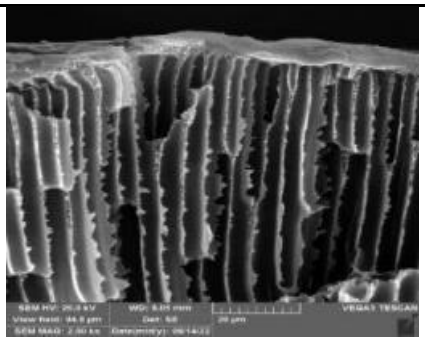

A) M0-0

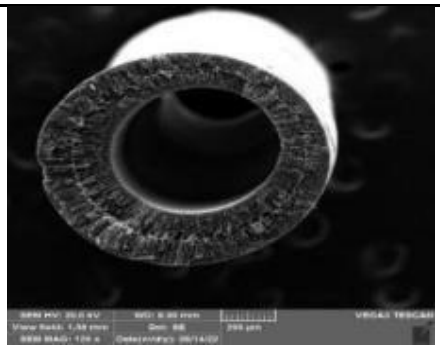

a) M0-0

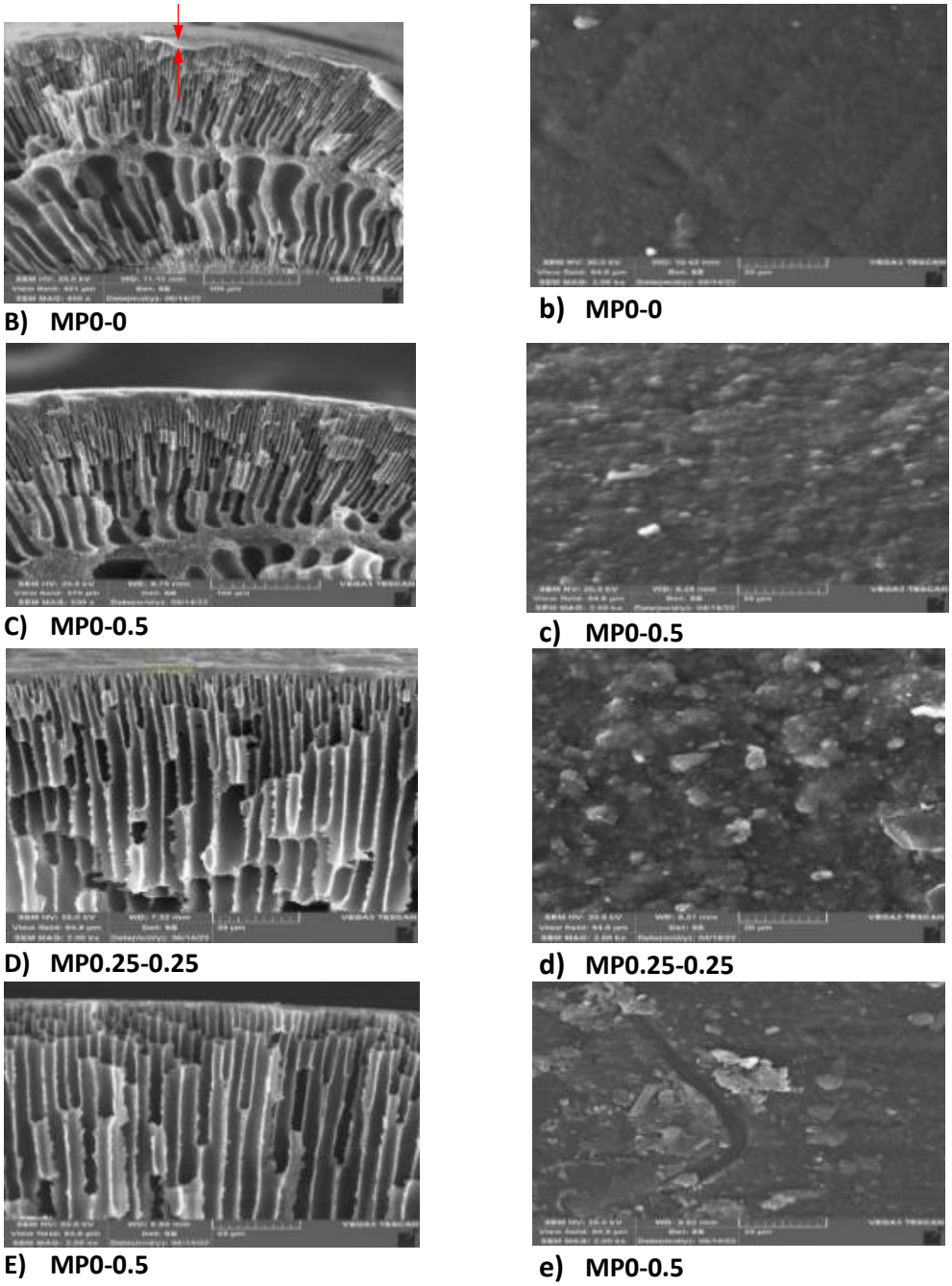

Figure 9 Surface SEM images magnified at ×5k and cross-sectional images magnified at ×2k

3.9 Performance Test Results of TFN Membranes

The water vapor permeability test was conducted at moisture levels of 2 to 6 bar gage. Figure 10 displays the results for selectivity, water vapor permeability, and nitrogen permeability at 60% relative humidity. With an ideal polymer-GO nanoparticle morphology, the nanosheet structure of GO enhances water vapor and nitrogen permeability. On the other hand, the hydrophilic nature of non-porous SiO_2 nanoparticles affects gas permeability differently, increasing water vapor solubility. The addition of SiO_2 is expected to enhance water vapor permeability. In the absence of defects and plasticization effects, membrane permeability generally decreases as pressure increases. This is because

defects form in the active layer of the membrane due to particle aggregation and the creation of a non-ideal void structure. Moreover, the plasticization effect, influenced by water's impact on secondary bonds, contributes to increase in permeability. When the selectivity decreases in comparison to the reference membrane, the rise in permeability under pressure is attributed to the primary factor. Conversely, when the selectivity compared to the neat membrane is enhanced, the increase in permeability under pressure is attributed to the secondary factor.

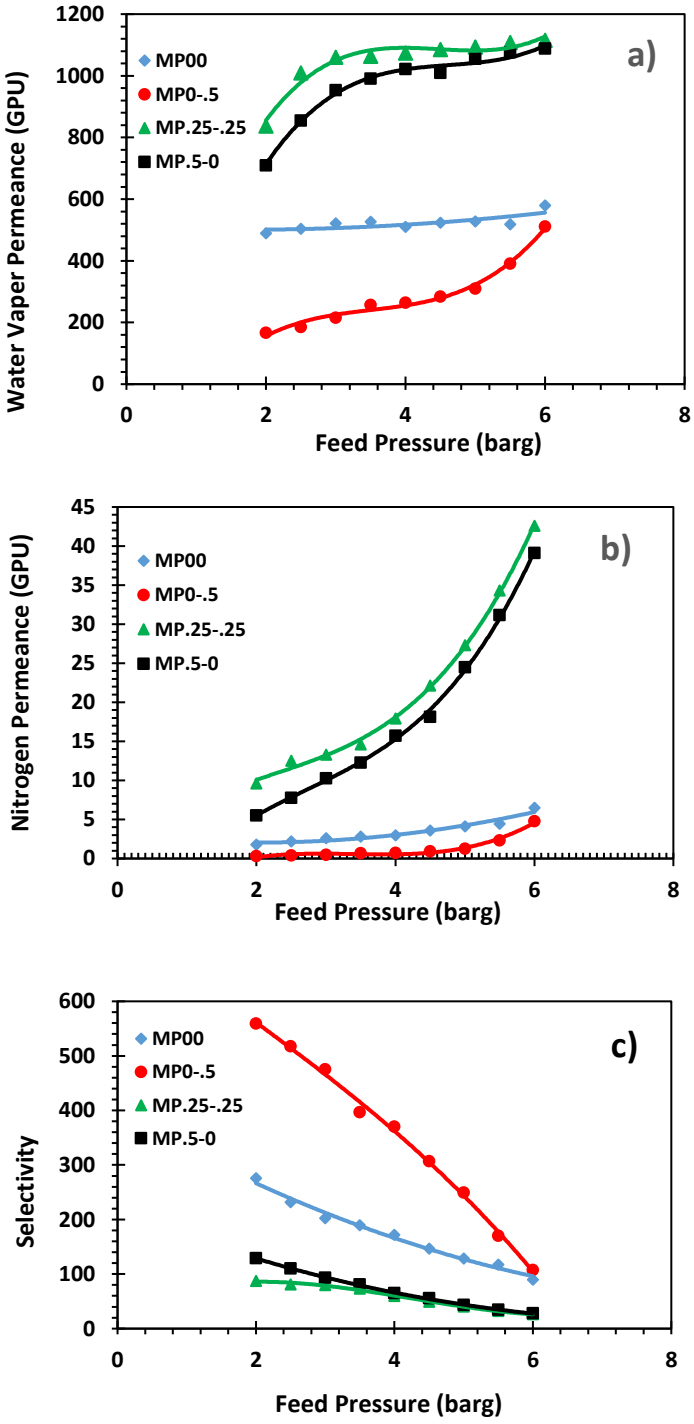

Figure 10 Trend of a) water vapor permeability, b) nitrogen permeability,and c) selectivity, of the fabricated membranes as a function of feed pressure (RH%= 60)

In the current study, the effect of pure nitrogen on polymer plasticization was found to be negligible. However, when wet feed gas permeability tests were conducted, a clear plasticization phenomenon was observed. Membranes containing GO, such as MP0.25-0.25 and MP0.5-0, had higher water vapor solubility due to the hydrophilicity of GO. The nano-sheet structure of GO also enhanced the permeation of nitrogen through water vapor, resulting in increased water vapor solubility and decreased nitrogen solubility. 0.5wt% of SiO_2 reduced both water vapor and nitrogen permeability, increasing selectivity. The presence of nanoparticles in the MP0.25-0.25 membrane further enhanced nitrogen permeability. Most likely, due to presence of the GO or SiO_2 nanoparticles specially the coexistence of nanoparticles, due to agglomeration of the nanoparticles a void morphology is probable to be formed, resulting in an increase in nitrogen permeability. Additionally, GO nanoparticles improved both water vapor solubility and nitrogen permeability, leading to increased overall permeability and decreased selectivity. Membrane MP0-0.5 was significantly impacted by the addition of SiO_2 nanoparticles, resulting in improved selectivity. SiO_2 nanoparticles impact morphology formation, affecting permeability and selectivity.

However, the MP0.5-0 membrane, with GO nanoparticles, saw an increase in water vapor and nitrogen permeability, leading to decreased selectivity. The likely cause of the nanoparticles' agglomeration is the primary reason for this phenomenon. GO tends to create void morphology due to agglomeration, while the distance between GO nanosheets can enhance leaking morphology. However, with increased loading, GO behavior in relation to SiO_2 reverses, leading to decreased selectivity and increased permeability. Conversely, an increase in SiO_2 loading leads to a shift from a void morphology to a leaking one. This can be explained by the tendency of GO nanoparticles to aggregate due to their high aspect ratio, in contrast to SiO_2 particles with a lower aspect ratio. It is noted that, the existence of the particle agglomeration was not detected in the SEM images provided, however it was proved by the gas permeation test as shown in Figure 10. According to Pourmohamedian *et al*. [25], silica nanoparticles display enhanced compatibility with Pebax1657 copolymer in comparison to titania nanoparticles. Based on the SEM micrographs' experimental findings (Figs. 9c to 9e), this phenomenon was also observed in the current study. Compounds with the highest selectivity exhibit superior morphology and synergy between nanoparticles, polymer, and water vapor, resulting in effective dehydration performance, like membrane MP0-0.5.

4.0 CONCLUSION

The performance of several GO-SiO_2/1657/Pebax PEI TFN membranes was investigated in the gas dehydration process in this study. These membranes, composed of PEI polymer with different percentages of graphene nanoparticles and silica oxide mixed with Pebax 1657 in the skin layer, demonstrated outstanding performance. The contact angle measurements suggested a heightened hydrophilicity of the created membranes, as there was a significant drop in the contact angle. The SEM images illustrated the formation of a uniform layer on the porous PEI substrate. The investigation revealed the influence of multiple factors on the dehydration properties of TFN membranes. The structure,

plasticization process, and hydrophilic properties all have crucial roles to play in this scenario. Additionally, the effectiveness of the system is dependent on the individual contribution of each nanoparticle. The influence of SiO_2 nanoparticles in their pure form is clearly demonstrated in the MP0-0.5 membrane. Upon introducing 0.5% of SiO_2 nanoparticles into the MP0-0.5 membrane, the morphology closely resembled the desired state due to the non-porous nature of SiO_2 and the relatively low concentration of nanoparticles. The reduction in water vapor and nitrogen permeability resulted in a higher selectivity ratio. The results of the ongoing research represent a crucial step forward in deepening our understanding of the complex mechanisms and phenomena involved in gas dehydration processes using TFN membranes. These findings are particularly valuable for industrial applications, as they offer a more comprehensive insight into the subject matter.

ACKNOWLEDGMENT

The authors express their heartfelt gratitude to the Sustainable Membrane Technology Research Group (SMTRG) at the Faculty of Petroleum, Gas and Petrochemical Engineering (FPGPE), Persian Gulf University (PGU), Iran, for their generous financial support. Additionally, the authors would like to acknowledge the National Iranian Gas Company (NIGC), Bushehr, for their kind financial assistance.

CONFLICTS OF INTEREST

The authors declare that there is no conflict of interest regarding the publication of this paper.

REFERENCES

[1] A. Tabe-Mohammadi. (1999). A review of the applications of membrane separation technology in natural gas treatment. *Separation Science and Technology, 34*(10), 2095-2111.

[2] A. Smith and J. Klosek. (2001). A review of air separation technologies and their integration with energy conversion processes. *Fuel Processing Technology, 70*(2), 115-134.

[3] D. Aaron and C. Tsouris. 2005. Separation of CO_2 from flue gas: a review. *Separation Science and Technology, 40*(1-3), 321-348.

[4] S. A. S. C. Samarasinghe. (2019). Development of ternary-component mixed-matrix membranes for advanced gas separations. Thesis. Nanyang Technological University, Singapore.

[5] L. Y. Ng, A. W. Mohammad, C. P. Leo, and N. Hilal. (2013). Polymeric membranes incorporated with metal/metal oxide nanoparticles: A comprehensive review. *Desalination, 308*, 15-33.

[6] S. A. Hashemifard, A. Khosravi, F. Abdollahi, Z. Alihemati, and M. Rezaee. 2020. Synthetic polymeric membranes for gas and vapor separations. *Synthetic Polymeric Membranes for Advanced Water Treatment, Gas Separation, and Energy Sustainability*, Elsevier, 217-272.

[7] F. Binci, F. E. Ciarapica, and G. Giacchetta. (2003). Natural gas dehydration in offshore rigs: Comparison between traditional glycol plants and innovative membrane systems. *Int Membr Sci Technol Conf.*

[8] H. Lin *et al.* (2012). Dehydration of natural gas using membranes.

Part I: Composite membranes. *Journal of Membrane Science, 413*, 70-81.

[9] H. Lin *et al.* (2013). Dehydration of natural gas using membranes. Part II: Sweep/countercurrent design and field test. *Journal of Membrane Science, 432*, 106-114,

[10] S. Hashemifard, M. Abdulhameed, E. Ghaderi, Z. Alihemati, and A. Ismail. 2023. Parametric and modelling study of H_2O-induced plasticization in PEI-TFC membrane for gas dehydration. *Separation and Purification Technology, 314*, 123564.

[11] J. R. Du, L. Liu, A. Chakma, and X. Feng. (2010). Using poly (N , N-dimethylaminoethyl methacrylate)/polyacrylonitrile composite membranes for gas dehydration and humidification. *Chemical Engineering Science, 65*(16), 4672-4681.

[12] H. Chen *et al.* (2018). An experimental study of membranes for capturing water vapor from flue gas. *Journal of the Energy Institute, 91*(3), 339-348.

[13] H. Cong, M. Radosz, B. F. Towler, and Y. Shen. (2007). Polymer–inorganic nanocomposite membranes for gas separation. *Separation and purification technology, 55*(3), 281-291.

[14] M. Aroon, A. Ismail, T. Matsuura, and M. Montazer-Rahmati. (2010). Performance studies of mixed matrix membranes for gas separation: A review. *Separation and purification Technology, 75*(3), 229-242.

[15] M. Zahid, A. Rashid, S. Akram, Z. A. Rehan, and W. Razzaq. (2018). A comprehensive review on polymeric nano-composite membranes for water treatment. *J. Membr. Sci. Technol., 8*(1), 1-20.

[16] M. Bassyouni, M. Abdel-Aziz , M. S. Zoromba, S. Abdel-Hamid, and E. Drioli. (2019). A review of polymeric nanocomposite membranes for water purification. *Journal of Industrial and Engineering Chemistry, 73*, 19-46,

[17] M. I. Baig, P. G. Ingole, W. K. Choi, S. R. Park, E. C. Kang, and H. K. Lee. (2016). Development of carboxylated TiO_2 incorporated thin film nanocomposite hollow fiber membranes for flue gas dehydration. *Journal of Membrane Science, 514*, 622-635.

[18] M. I. Baig, P. G. Ingole, J.-d. Jeon, S. U. Hong, W. K. Choi, and H. K. Lee. (2019). Water vapor transport properties of interfacially polymerized thin film nanocomposite membranes modified with graphene oxide and GO-TiO_2 nanofillers. *Chemical Engineering Journal, 373*, 1190-1202.

[19] J. H. Kim, S. Y. Ha, and Y. M. Lee. (2001). Gas permeation of poly (amide-6-b-ethylene oxide) copolymer. *Journal of Membrane Science, 190*(2), 179-193.

[20] G. Dennis and G. O Brien. (2000). Polyether block amide resins:" bridging the gap between thermoplastics and rubbers. *Papers-American Chemical Society Division of Rubber ChemistrY*, 21.

[21] J. Aburabie and K.-V. Peinemann. (201.). Crosslinked poly (ether block amide) composite membranes for organic solvent nanofiltration applications. *Journal of*

Membrane Science, 523, 264-272.

[22] Y. Yampolskii, L. Starannikova, N. Belov, M. Gringolts, E. Finkelshtein, and V. Shantarovich. (2010). Addition-type polynorbornene with Si $(CH_3)_3$ side groups: Detailed study of gas permeation, free volume and thermodynamic properties. *Membrane Gas Separation*, 43-57.

[23] F. H. Akhtar, M. Kumar, and K.-V. Peinemann. (2017). Pebax® 1657/Graphene oxide composite membranes for improved water vapor separation. *Journal of Membrane Science, 525*, 187-194.

[24] S. J. Poormohammadian, P. Darvishi, A. M. G. Dezfuli, and M. Bonyadi. (2018). Incorporation of functionalized silica nanoparticles into polymeric films for enhancement of water absorption and water vapor transition. *Fibers and Polymers, 19*(10), 2066-2079.

[25] S. J. Poormohammadian, P. Darvishi, and A. M. G. Dezfuli. (2019). Enhancing natural gas dehydration performance using electrospun nanofibrous sol-gel coated mixed matrix membranes. *Korean Journal of Chemical Engineering, 36*(6), 914-928.

[26] Y. Liu *et al.* (2019). Synthesis of novel high flux thin-film nanocomposite nanofiltration membranes containing GO–SiO_2 via interfacial polymerization. *Industrial & Engineering Chemistry Research, 58*(49), 22324-22333,

[27] M.-C. Hsiao *et al.* (2013). Thermally conductive and electrically insulating epoxy nanocomposites with thermally reduced graphene oxide–silica hybrid nanosheets. *Nanoscale*, 5(13), 5863-5871.

[28] M. Sheikh, M. Asghari, and M. Afsari. (2018). Effect of tiny amount of zinc oxide on morphological and thermal properties of nanocomposite PEBA thin films. *Alexandria Engineering Journal, 57*(4), 3661-3669.

[29] N. Norahim, K. Faungnawakij, A. T. Quitain, and C. Klaysom. (2019). Composite membranes of graphene oxide for CO_2/CH_4 separation. *Journal of Chemical Technology & Biotechnology, 94*(9), 2783-2791.

[30] Behzad Kord1 Mohammad Dahmardeh Ghalehno·Farnaz Movahedi1. (2020). Effect of surface functionalization of SiO_2 nanoparticles on the dynamic mechanical, thermal and fire properties of wheat straw/LDPE composites. *Journal of Polymers and the Environment, 28*, 304-316.

[31] Adikwu Gowon Jacob1,2,3 and Roswanira Abdul Wahab. (2022). Preliminary studies and characterization of oil palm frond leaves silica-based bonded lipase. *Science Letters, 16*(2).

[32] M. S. Abdul Wahab, S. Abd Rahman, and R. Abu Samah. (2021). Super selective dual nature GO bridging PSF-GO-Pebax thin film nanocomposite membrane for IPA dehydration. *Polymer-Plastics Technology and Materials, 60*(6), 670-679.

[33] R. S. Murali, A. Ismail, M. Rahman, and S. Sridhar. (2014). Mixed matrix membranes of Pebax-1657 loaded with 4A zeolite for gaseous separations. *Separation and Purification Technology, 129*, 1-8.